Appearance and Dynamics of Helical Flux Tubes under Electron Cyclotron Resonance Heating in the Core of KSTAR Plasmas

G. S. Yun,[1,*] H. K. Park,[1] W. Lee,[1] M. J. Choi,[1] G. H. Choe,[1] S. Park,[2] Y. S. Bae,[2] K. D. Lee,[2] S. W. Yoon,[2] Y. M. Jeon,[2] C. W. Domier,[3] N. C. Luhmann, Jr.,[3] B. Tobias,[4] A. J. H. Donné,[5,6] and KSTAR Team[2]

[1]*POSTECH, Pohang 790-784, Korea*
[2]*National Fusion Research Institute, Daejeon 169-148, Korea*
[3]*University of California, Davis, California 95616, USA*
[4]*Princeton Plasma Physics Laboratory, Princeton, New Jersey 08543, USA*
[5]*Dutch Institute for Fundamental Energy Research, Nieuwegein, The Netherlands*
[6]*Eindhoven University of Technology, Eindhoven, The Netherlands*

(Received 20 September 2011; published 3 October 2012)

Dual (or sometimes multiple) flux tubes (DFTs) have been observed in the core of sawtoothing KSTAR tokamak plasmas with electron cyclotron resonance heating. The time evolution of the flux tubes visualized by a 2D electron cyclotron emission imaging diagnostic typically consists of four distinctive phases: (1) growth of one flux tube out of multiple small flux tubes during the initial buildup period following a sawtooth crash, resulting in a single dominant flux tube along the $m/n = 1/1$ helical magnetic field lines, (2) sudden rapid growth of another flux tube via a fast heat transfer from the first one, resulting in approximately identical DFTs, (3) coalescence of the two flux tubes into a single $m/n = 1/1$ flux tube resembling the internal kink mode in the normal sawteeth, which is explained by a model of two current-carrying wires confined on a flux surface, and (4) fast localized crash of the merged flux tube similar to the standard sawtooth crash. The dynamics of the DFTs implies that the internal kink mode is not a unique prerequisite to the sawtooth crash, providing a new insight on the control of the sawtooth.

DOI: 10.1103/PhysRevLett.109.145003 PACS numbers: 52.30.Cv, 52.35.Vd, 52.55.Fa, 52.70.Gw

The sawtooth phenomena commonly observed in the toroidally confined plasmas are periodic relaxation events characterized by fast collapse of the heat slowly built in the core region. The relaxation process called sawtooth crash is generally believed to be triggered by the onset of a magnetohydrodynamic (MHD) instability called internal kink mode having $m/n = 1/1$ helicity, where m and n are poloidal and toroidal mode numbers, respectively. Despite its simple spatial mode structure, it is well recognized [1] that even the linear stability of the internal kink mode involves rich physics including macroscopic fluid effects, kinetic effects of both thermal and nonthermal particles, and nonideal local effects around the $q = m/n = 1$ magnetic flux surface such as resistivity, finite ion Larmor radius, and diamagnetic drifts. The nonlinear stages of the sawtooth following the onset of the internal kink involves diverse phenomena such as saturated kink, incomplete relaxation (also known as partial crash), and nonaxisymmetric localized crash.

The control methods for sawteeth have been investigated extensively for several decades because uncontrolled sawtooth crashes can trigger other harmful instabilities such as neoclassical tearing modes and edge localized modes, which can lead to confinement loss and damage on the first wall [2]. Several effective methods have been demonstrated such as electron cyclotron resonance heating (ECH) [3–6] and generation of energetic ions using neutral beam injection [7,8] or ion cyclotron waves [9].

During the 2010 and 2011 experiments in the KSTAR (Korea Superconducting Tokamak Advanced Research) device [10], a superconducting tokamak designed for steady-state operation, the effect of ECH on the sawtooth dynamics has been studied in 2D using an advanced imaging technique for local electron temperature (T_e) measurements called electron cyclotron emission imaging (ECEI). The KSTAR ECEI system [11], built on the remarkable scientific contributions from the previous generation ECEI systems [12,13] and technological innovations [14,15], provides a pair of 24(vertical) $\times$ 8(radial) local T_e measurements in the same poloidal cross section with a spatial resolution $\sim$1–2 cm and a time resolution $\sim 1\ \mu$s as schematically shown in Fig. 1(a).

Interestingly, a new variation of sawtooth instability distinct from the internal kink mode of the normal sawteeth has been commonly observed during the ECH injection period for a wide variety of operation regimes, i.e., different shaping (elongation $\kappa = 1$–1.8), heating (with or without neutral beam injection), or confinement regime (low or high). Unlike the internal $m = 1$ kink displacement of the entire core region ($q < 1$), the new instability is characterized by dual $m/n = 1/1$ filamentary hot flux tubes near the $q = 1$ surface during both the initial buildup phase (the time period with increasing core T_e) and the precursor phase preceding the sawtooth crash. A hint for the generation mechanism of the dual flux tubes (DFTs) has been obtained by examining a large number of discharges

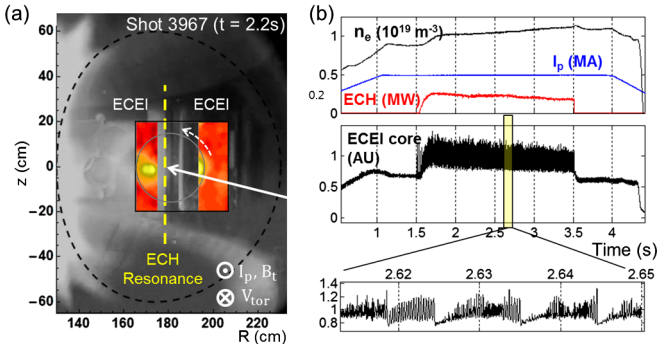

FIG. 1 (color online). (a) Visible camera image of a plasma with 110 GHz ECH (shot 3967). The inset images are the DFTs captured by the ECEI. The white arrow is the approximate ECH beam path, whose second harmonic resonance was on the magnetic axis ($R = 1.8$ m). As indicated, the toroidal magnetic field (B_t) and the plasma current (I_p) were both out of the plane and the toroidal plasma rotation (V_{tor}) was into the plane (i.e., countercurrent direction). (b) Time traces of I_p, heating power, line-averaged electron density (n_e), and ECE intensity. The highlighted zoomed view shows the characteristic time trace of the DFTs.

(~ 700). The DFTs were observed only in the discharges with ECH and predominantly when both of the following ECH conditions were satisfied: (1) the resonance position is within the $q = 1$ radius and (2) the injection angle is perpendicular or co-current, i.e., not countercurrent. These may suggest that the modified current profile or suprathermal electrons in the core region due to ECH play an important role in the DFTs generation. Although the DFTs are the most prominent feature of the KSTAR ECH plasmas, other related structures were also observed such as triple hot flux tubes and a crescent-shaped hot structure, a detailed description of which is beyond the scope of this Letter.

In the presence of DFTs, neither the internal kink nor a substantial heat accumulation was observed at the plasma core. The crash was delayed until the two flux tubes merged and became like the internal kink mode of the normal sawteeth, which will be described later in detail. This observation implies that the DFTs delay the onset of the sawtooth relaxation crash and the generation of DFTs may be considered as a mechanism for controlling the sawtooth period and/or crash amplitude. Similar prevention or stabilization of neoclassical tearing modes may be possible too if ECH can induce similar filamentation near $q = 2$ flux surface. In particular, the DFTs under ECH may have a critical implication to tokamaks like ITER where ECH will be a major heating and current drive tool for the core plasmas.

It is illuminating to compare DFTs with other nonstandard sawtooth-related phenomena with or without ECH. (1) The phenomenon *frequency doubling* [4,5], which may indicate the existence of DFTs, was often found in the precursor phase of the so-called saturated sawteeth during localized ECH. However, the frequency doubling was not given much attention, presumably because it would have been very difficult to understand the generation and merging dynamics of the DFTs, which are clearly visualized by the 2D ECEI in this Letter, from the conventional 1D diagnostics such as ECE radiometry and soft x-ray measurements. (2) The electron fishbone instability [16] is a modified internal kink mode which can be excited by barely trapped suprathermal electrons generated by ECH. This instability is characterized by intermittent growth and decay of a single $m = 1$ internal kink mode, which is clearly different from the DFTs. (3) Multipeaked electron temperature (T_e) profiles were observed in the sawtoothing core of several tokamaks [17,18] and interpreted as a result of a macroscopic magnetic island and localized ECH along the island's outer flux surface [18]. Such interpretation would suggest a large magnetic island and snakelike hot temperature band in the 2D ECEI data, which is different from the DFTs. (4) Higher mode number MHD instabilities (in particular, the $m/n = 2/2$ mode) were found during the sawtooth crashes of Ohmically heated plasmas [19–21]. In these studies, the higher order modes were only observed in the vicinity of the crash phase whereas the DFTs in the present work are observed throughout all phases of sawtooth. It should be also noted that a simple $m/n = 2/2$ mode alone cannot explain the coalescence of the DFTs.

These phenomenological comparisons suggest that thermal and/or suprathermal electrons heated by ECH waves can alter the core MHD environment in a different way than previously known. The dynamics of DFTs are described below in detail to emphasize the newly identified effects of ECH.

Figure 1(a) is a visible camera image of a plasma with on-axis ECH resonance with the inset core ECEI images showing DFTs. Figure 1(b) is the time traces of several key plasma parameters including the core ECEI signal which shows the significant increase of the core MHD activity caused by ECH. The zoomed ECEI time trace shows the sawtoothlike patterns with a period ~ 10 ms. Note the early appearance of oscillations in the buildup phase, which is a stark difference compared to normal sawteeth where the precursor oscillation develops after the buildup phase and near the crash.

A typical sawtooth pattern with DFTs is illustrated by a detailed time trace of core ECE signal in Fig. 2, showing the early appearance of the precursor oscillation and the sudden doubling of the oscillation frequency. In the ECEI images, the frequency doubling corresponds to the emergence of a second hot flux tube as indicated by the arrows. Note that the time trace in Fig. 2 is only one example among many other observed patterns exhibiting diverse combinations of the state of *single* flux tube and the state of DFTs in one sawtooth period. A few examples

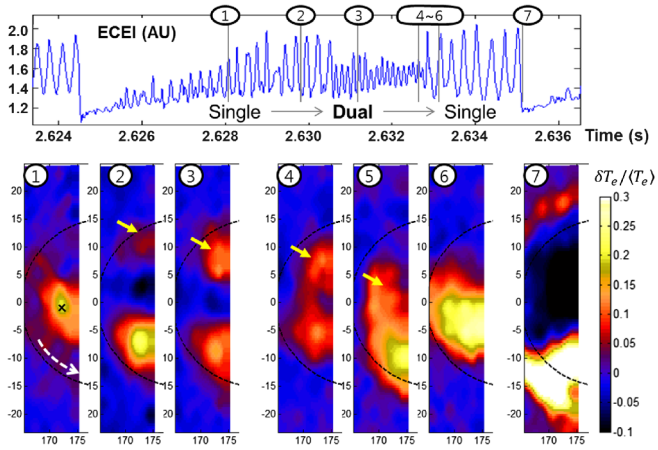

FIG. 2 (color online). (Top) Time trace of an ECEI channel (indicated by the cross mark in the frame 1 below) showing a typical sawtooth pattern with DFTs. (Bottom) ECEI images of the DFTs at the selected times. The flux tubes rotate counterclockwise as indicated by the dashed arrow. The short arrows indicate the sudden growth of the second flux tube. The dashed circles represent the approximate location of the $q = 1$ surface inferred from the inversion radius of the crash phase image (frame 7).

include (single → dual → single → partial crash → single → crash), (dual → single → dual → single → crash), and (dual → single → dual → crash). The observed ordering among the *single* and *dual* states is random.

The first stage of the evolution is a growth of multiple (1–3) filamentary hot flux tubes in the core in the early buildup phase following a sawtooth crash. Typically, one flux tube grows fast and becomes dominant, while all the others disappear or one of them remains very faint. Note that a smaller hot flux tube often survives, located approximately at the opposite side of the dominant flux tube (see frame 2), and becomes the seed to the next stage. The dominant flux tube has $m/n = 1/1$ helicity, indicating that it is formed along the $q = 1$ local magnetic field line. The observed counterclockwise rotation of the flux tube in the frame of the ECEI view (indicated by the white dashed arrow in frame 1) is consistent with a rigid body rotation of the flux tube due to the toroidal plasma rotation ~4 kHz.

The second stage (frames 2–3 of Fig. 2) is a rapid growth of the second hot flux tube of the same helicity resulting in the state of DFTs as shown by the enlarged time trace and the model figures in Fig. 3. The time trace includes an ECE radiometer signal toroidally separated by 3/16 of the circumference (67.5° apart) to show that the time delay between the two signals (~ 0.05 ms) with respect to the oscillation period (~0.3 ms for individual flux tubes) is consistent with the $n = 1$ mode structure of the flux tubes. The growth of the small seed flux tube has three interesting features. (1) The growth time scale $\lesssim 100$ μs, is much shorter than the resistive diffusion time $\tau_\eta = \mu_0 r_1^2/\eta \sim 1$ s but much longer than the Alfvén

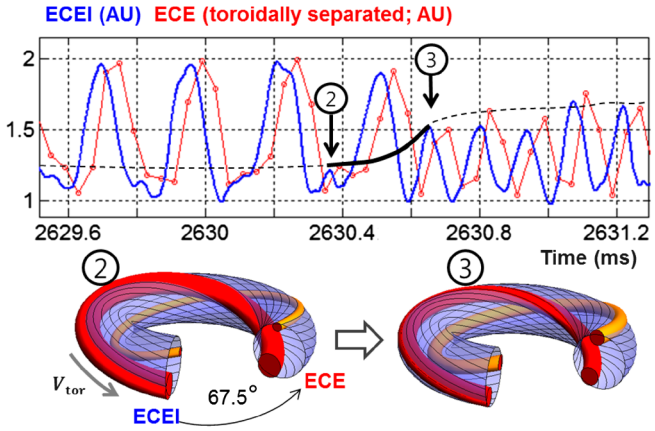

FIG. 3 (color online). Growth of the second flux tube. The dashed curve traces the sudden rapid growth of the second flux tube as indicated by the arrows coinciding with the diminishment of the first flux tube. This process is schematically illustrated by the flux tube models below. The thick (blue) curve is the ECEI signal and the thin (red) curve with small open circles is the corresponding ECE radiometer signal toroidally separated by 3/16 of the circumference at the same radial location.

time $\tau_A = r_1/v_A \sim 1$ μs and the parallel transit time of thermal electrons $\tau_{th} \sim 1$ μs, where r_1 is the radius of $q = 1$ surface, η is the Spitzer resistivity, and v_A is the poloidal Alfvén speed. (2) The growth of the second flux tube occurs simultaneously with the reduction of the first flux tube; i.e., the integrated sum of the ECE intensities of the two flux tubes remains approximately constant. This observation excludes the secondary heating of a macroscopic magnetic island [18] as a possible mechanism for the generation of the second flux tube. (3) The two flux tubes typically become balanced and maintain their relative positions while co-rotating inside the $q = 1$ surface (dashed circle in Fig. 2, which is inferred from the crash phase). The two balanced flux tubes (i.e., DFTs) could be two separate $m/n = 1/1$ modes or an $m/n = 2/2$ mode. The fast heat exchange between the flux tubes needs further investigation for possible mechanisms such as a transient localized magnetic reconnection between two $m/n = 1/1$ flux tubes (in the former case) or a mode conversion from $m/n = 1/1$ to $2/2$ mode (in the latter case). The duration of the DFT state varies from less than ~1 to ~10 ms.

The third stage (frames 4–6 of Fig. 2) is a coalescence of the two flux tubes into a single large hot core on a time scale $\lesssim 100$ μs. The observed merge process, as schematically illustrated in Fig. 4, is a gradual attraction of the flux tubes in the poloidal direction rather than radial direction (i.e., the motion is approximately confined on the flux surface). This is not consistent with a mode conversion from $m/n = 2/2$ to $1/1$ mode, indicating that the two flux tubes are two separate $m/n = 1/1$ modes. It is not clear whether the merging process is helically symmetric or asymmetric. In either case, the end of the merging is a

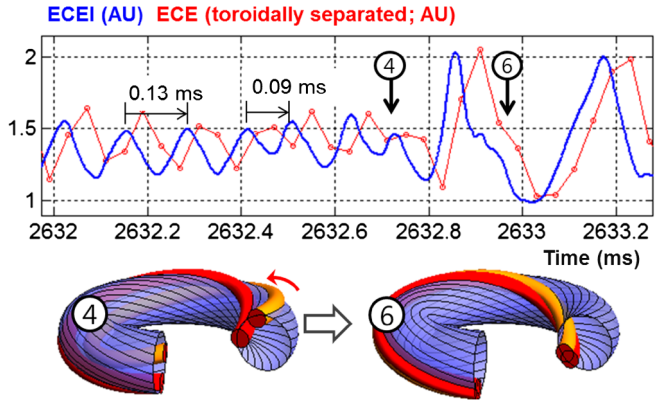

FIG. 4 (color online). Coalescence of the dual helical flux tubes. Before merge, the second flux tube (orange in the model) catches the first flux tube (red in the model) as indicated by the shortening of the time separation between the two flux tubes. The merging (4 → 6) completes in ~100 μs.

single helically symmetric flux tube, resembling the $m = 1$ internal kink mode of the typical tearing type sawtooth instability. The final stage (frame 7) is the crash, i.e., the relaxation of the core heat. The heat transport during the crash is fast (< 100 μs), collective, and localized, identical to the previously observed sawtooth crash [12].

During the merge process, the apparent rotation frequencies of the two $m/n = 1/1$ flux tubes are observed to vary as shown in Figs. 5(a) and 5(c) In addition, the apparent rotation frequency typically changes from one DFT state to the next DFT state in the case of multiple DFT states as shown in Fig. 5(b). Note also that the frequency of the DFT state is often not exactly double the frequency of the single flux tube state. These observations imply that the flux tubes during the DFT state have a net poloidal rotation because the toroidal plasma rotation is unlikely to change appreciably during the time scale ~1 ms. The net poloidal rotation

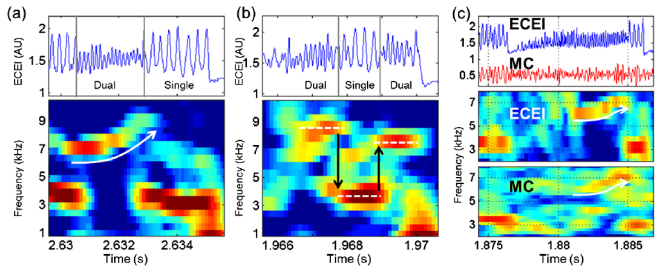

FIG. 5 (color online). Rotation velocities of the flux tubes. (a) Frequency transitions for a typical sawtooth pattern with DFTs, single → dual(frequency doubling) → single → crash. The core rotation accelerated during the merge process as indicated by the arrow. (b) Another example of frequency transitions, dual → single → dual → crash. The horizontal dashed lines are at 8.5, 3.7, and 7.4 kHz, respectively. (c) Comparison between the ECEI signal and a Mirnov coil [MC; dB_z/dt (AU)] signal.

may be explained by a centrifugal attraction of the two helical flux tubes confined in a guiding magnetic flux surface if the flux tubes carry an additional current on top of the average axisymmetric plasma current:

$$F = \mu_0 \frac{\Delta I_1 \Delta I_2}{2\pi d} = M_1 r_1 \omega^2 = M_2 r_2 \omega^2, \qquad (1)$$

where the subscript denotes individual flux tubes, F is the centrifugal attractive force per unit length, the ΔI's are the additional current defined by $\Delta I \equiv A_{\rm tube}(J_{\rm tube} - J_q)$ (here the J_q is the average current density on the flux surfaces surrounding the flux tube and $J_{\rm tube}$ is the average current density inside the flux tube, and $A_{\rm tube}$ is the cross-sectional area of the flux tube), d is the radial distance between the tubes, the M's are the mass per unit length, the r's are the distance from the center of mass, and ω is the centrifugal orbiting frequency, i.e., the net poloidal angular frequency. The observed change in the rotation frequency, $\Delta f \sim 1.5$ kHz, corresponds to the net poloidal rotation caused by the attraction, i.e., $\omega = 2\pi\Delta f$. For the balanced flux tubes as described previously, $\Delta I^2 = M\pi d^2\omega^2/\mu_0$ where $M = M_1 = M_2$ and $\Delta I = \Delta I_1 = \Delta I_2$, which yields $\Delta I \sim 100$ A using the observed $\Delta f \sim 1.5$ kHz, $d \sim 25$ cm, and $M = nm_i\pi a^2$ with the core ion density $n \sim 2 \times 10^{19}$ m^{-3}, the deuterium ion mass for m_i, and the tube radius $a \sim 3$ cm. The corresponding additional current density ~3.5 A/cm^2 is a few % of the average current density inside the $q = 1$ surface (~ 150 A/cm^2).

In Fig. 5(c), the comparison of the frequency spectrum between the ECEI signal and an Mirnov coil (MC) signal [22], which measures the time-varying magnetic fields (dB/dt), supports that the flux tubes are indeed $m/n = 1/1$ helical current perturbations rotating in the lab frame. However, a quantitative confirmation of such small localized current perturbation by the conventional current profile diagnostics based on the motional Stark effect or the Faraday rotation would be difficult due to the weakness of each technique (in the temporal and the spatial resolution, respectively). Instead, a numerical simulation would be necessary to investigate the role of the additional current in the formation of DFT and subsequent dynamics similar to the investigation of triple tearing modes due to the current perturbations near the $q = 1$ surface [23]. The use of MC signals to determine the perturbed current profile [24] might also become possible if the effect of wall currents induced around the MC probes could be modeled accurately.

Note that there is insignificant bending of the main toroidal field component during the merging process because of the $m/n = 1/1$ field line geometry of the flux tubes, which leads to the observed complete merge in contrast to the experiment on the line-tied current-carrying flux ropes [25], where the initially attracting two flux ropes were observed to rebound due to the restoring bending force of the equilibrium field lines. As the two flux tubes

approach to each other close enough, a magnetic reconnection will be inevitable and result in the complete coalescence, similar to the coalescence of current-carrying solar coronal loops [26].

In summary, the dual $m/n = 1/1$ hot flux tubes in the core of the tokamak plasmas with ECH have been observed in 2D using the ECEI diagnostic. The spatial structure and dynamics of the DFTs are different from the internal kink mode and other previous observations of the $m/n = 2/2$ mode. The merging of the DFTs, which may be explained by the mutual attraction between the flux tubes carrying additional currents, results in a structure similar to the internal kink mode and ultimately leads to the relaxation crash. Although the exact generation mechanism is not clear at this point, the DFTs imply the existence of an instability mode distinct from the internal kink mode or its known variations, opening up a new insight on the control of MHD instabilities using ECH.

This work was supported by the NRF Korea under the Contract No. 20110018724 and the BK21 program, the U.S. DOE, and the Association Euratom-FOM.

*gunsu@postech.edu

[1] F. Porcelli, D. Boucher, and M. N. Rosenbluth, Plasma Phys. Controlled Fusion **38**, 2163 (1996).
[2] I. T. Chapman, Plasma Phys. Controlled Fusion **53**, 013001 (2011).
[3] K. Hanada *et al.*, Phys. Rev. Lett. **66**, 1974 (1991).
[4] A. Pochelon *et al.*, Nucl. Fusion **39**, 1807 (1999).
[5] I. Furno *et al.*, Nucl. Fusion **41**, 403 (2001).
[6] C. Angioni, T. P. Goodman, M. A. Henderson, and O. Sauter, Nucl. Fusion **43**, 455 (2003).
[7] I. T. Chapman, I. Jenkins, R. V. Budny, J. P. Graves, S. D. Pinches, S. Saarelma, and JET EFDA Contributors, Plasma Phys. Controlled Fusion **50**, 045006 (2008).
[8] I. T. Chapman, M. F. de Bock, S. D. Pinches, M. R. Turnyanskiy, V. G. Igochine, M. Maraschek, and G. Tardini, Phys. Plasmas **16**, 072506 (2009).
[9] J. P. Graves, I. Chapman, S. Coda, L. G. Eriksson, and T. Johnson, Phys. Rev. Lett. **102**, 065005 (2009).
[10] G. S. Lee *et al.*, Nucl. Fusion **40**, 575 (2000).
[11] G. S. Yun *et al.*, Rev. Sci. Instrum. **81**, 10D930 (2010).
[12] H. K. Park, N. C. Luhmann, Jr., A. J. H. Donné, I. G. J. Classen, C. W. Domier, E. Mazzucato, T. Munsat, M. J. van de Pol, and Z. Xia, Phys. Rev. Lett. **96**, 195003 (2006).
[13] I. G. J. Classen *et al.*, Phys. Rev. Lett. **98**, 035001 (2007).
[14] B. Tobias *et al.*, Rev. Sci. Instrum. **80**, 093502 (2009).
[15] B. Tobias *et al.*, Rev. Sci. Instrum. **81**, 10D928 (2010).
[16] K. Wong *et al.*, Phys. Rev. Lett. **85**, 996 (2000).
[17] G. Cima, K. W. Gentle, A. Wootton, D. L. Brower, L. Zeng, B. H. Deng, C. W. Domier, and N. C. Luhmann Jr., Plasma Phys. Controlled Fusion **40**, 1149 (1998).
[18] F. Porcelli, E. Rossi, G. Cima, and A. Wootton, Phys. Rev. Lett. **82**, 1458 (1999).
[19] Y. Nagayama, G. Taylor, M. Yamada, E. D. Fredrickson, A. C. Janos, and K. M. McGuire, Nucl. Fusion **36**, 521 (1996).
[20] S. Yamaguchi, H. Igami, H. Tanaka, and T. Maekawa, Plasma Phys. Controlled Fusion **46**, 1163 (2004).
[21] X. Xu *et al.*, Plasma Phys. Controlled Fusion **52**, 015008 (2010).
[22] S. G. Lee and J. G. Bak, Rev. Sci. Instrum. **72**, 439 (2001).
[23] A. Bierwage, S. Hamaguchi, M. Wakatani, S. Benkadda, and X. Leoncini, Phys. Rev. Lett. **94**, 065001 (2005).
[24] M. Kikuchi, Nucl. Fusion **26**, 101 (1986).
[25] X. Sun, T. P. Intrator, L. Dorf, J. Sears, I. Furno, and G. Lapenta, Phys. Rev. Lett. **105**, 255001 (2010).
[26] T. Tajima, J. Sakai, H. Nakajima, T. Kosugi, F. Brunel, and M. R. Kundu, Astrophys. J. **321**, 1031 (1987).